

Sandeel (*Ammodytes marinus*) larval transport patterns in the North Sea from an individual-based hydrodynamic egg and larval model

Asbjørn Christensen, Henrik Jensen, Henrik Mosegaard, Mike St. John, and Corinna Schrum

Abstract: We have calculated a time series of larval transport indices for the central and southern North Sea covering 1970–2004, using a combined three-dimensional hydrodynamic and individual-based modelling framework for studying sandeel (*Ammodytes marinus*) eggs, larval transport, and growth. The egg phase is modelled by a stochastic, nonlinear degree-day model describing the extended hatch period. The larval growth model is parameterized by individually back-tracking the local physical environment of larval survivors from their catch location and catch time. Using a detailed map of sandeel habitats in the North Sea, the importance of hydrography for early life stages of sandeel to their recruitment success is explored. We find that the sandeel larval transport patterns in the North Sea are relatively robust toward uncertainties in biological parameters, when mortality aspects are included. We find only weak spatiotemporal correlations between elements of the transport indices in the time series, mainly positive correlation between retention terms for the same year. The transport connectivity of sandeel habitats in the North Sea and the dynamical properties of the North Sea transport system are also analyzed, and we introduce novel a scheme to quantify direct and indirect connectivity on equal footings in terms of an interbank transit time scale.

Résumé : Nous avons calculé une série chronologique d'indices de transport des larves pour les régions centrale et australe de la mer du Nord pour la période 1970–2004 à l'aide d'un cadre de modélisation hydrodynamique tridimensionnel et basé sur l'individu, afin d'étudier le transport et la croissance des oeufs et des larves du lançon (*Ammodytes marinus*). La phase des oeufs peut se représenter par un modèle stochastique non linéaire de degrés-jours qui décrit la période prolongée de l'éclosion. Les paramètres du modèle de croissance larvaire s'obtiennent en retraçant l'environnement physique local individuel des larves survivantes à partir du lieu et du moment de leur capture. Une carte détaillée des habitats des lançons dans la mer du Nord permet d'explorer l'importance de l'hydrographie chez les premiers stades de vie des lançons pour le succès du recrutement. Nous observons que les patrons de transport des larves de lançons dans la mer du Nord sont relativement robustes vis-à-vis les incertitudes des variables biologiques lorsqu'on tient compte des aspects de la mortalité. Il n'existe que de faibles corrélations spatio-temporelles entre les éléments des indices de transport dans la série chronologique, principalement des corrélations positives entre les différents termes de la rétention dans une même année. Nous analysons aussi la connectivité des habitats par le transport de lançons dans la mer du Nord et les propriétés dynamiques du système de transport de la mer du Nord; nous présentons une méthode inédite pour calculer les connectivités directe et indirecte sur une base égale sur l'échelle du temps de passage d'un banc à un autre.

[Traduit par la Rédaction]

Introduction

The lesser sandeel (*Ammodytes marinus*) plays a pivotal role as a midtrophic wasp-waist component in the North Sea ecosystem and is the basis for an important fishery. After metamorphosis from larvae to juveniles, the sandeels settle, i.e., they bury in the sediment during times when they do not feed on zooplankton (see, e.g., Winslade 1971). Sandeels are assumed to remain resident on sandbank habitats (Kunzlik et al. 1986). North Sea lesser sandeels spawn

in midwinter and the eggs stick to the sand grains at the seabed until hatch (Macer 1966). The relatively short larval drift phase of 1–3 months (Wright 1993; Wright and Bailey 1996; Jensen 2001) in February to May is believed to render the sandeel recruitment rather sensitive to optimal hydrographic conditions (Wright and Bailey 1996).

Present sandeel stock-assessment models treat the North Sea sandeel populations as one single homogeneous stock or, at most, two stocks. These stock-assessment models neither predict stock variations sufficiently well nor provide a

Received 15 March 2007. Accepted 23 January 2008. Published on the NRC Research Press Web site at cjfas.nrc.ca on 25 June 2008. J19888

A. Christensen,¹ H. Jensen, H. Mosegaard, and C. Schrum.² Danish Institute for Fisheries Research, Afd. for Havfiskeri, Charlottenlund Slot, 2920 Charlottenlund, Denmark.

M. St. John. Institute for Hydrobiology and Fisheries Science, Hamburg University, Olbersweg 24, 2767 Hamburg, Germany.

¹Corresponding author (e-mail: asc@difres.dk).

²Present address: Geophysical Institute, University of Bergen, Allégaten 70, N-5007 Bergen, Norway.

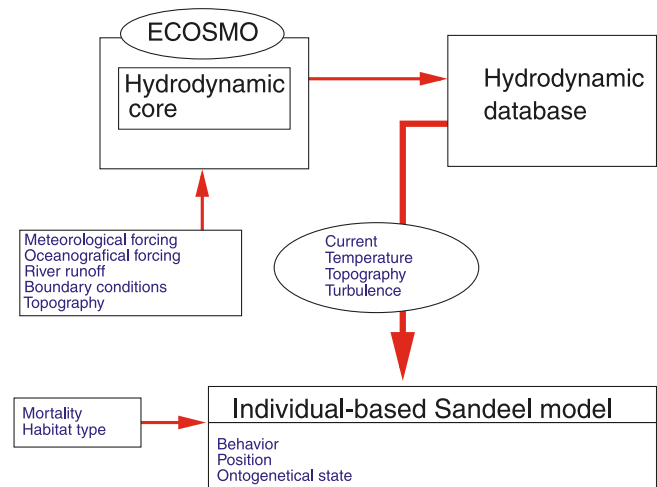
satisfactory starting point for linking population dynamics to underlying oceanographic and biological processes that are major drivers for the population dynamics of many fish species including sandeels (Arnott and Ruxton 2002). This detailed understanding appears highly important presently, when ecosystems face potential regime shifts triggered either directly by global warming or by cascade effects of global warming. Statistical models inferred from hindsight time series are uncertain when the dynamic regime of the ecosystems changes, because their forecasts are based on the past dynamics in a different regime. Alternative and potentially more powerful tools are based on deterministic modelling of underlying processes using invariant laws of nature.

Our working hypothesis is that spatially explicit population dynamics is necessary to improve the description of the stock–recruitment relationship for sandeels and that adult sandeel population survival and growth is regulated locally by spatially varying mortality and zooplankton availability. However, spatiality per se may trigger new effects not accessible in models without spatial freedom, like coexistence, patchiness, or fluctuations in the population distribution. On the biological side, we also test hypotheses about the importance of variable, extended hatch periods (compared with a fixed day) and hypotheses about the mechanism controlling the juvenile settlement process (a flexible settlement schedule compared with a fixed body length trigger), and finally, we test hypotheses about the impact of exogene and endogene factors on larval growth.

Earlier hydrodynamic studies of sandeel larval transport already have stressed the importance of advective transport. Berntsen and co-workers (Berntsen et al. 1994) considered a long time series for passive advection in the North Sea but had no integrated larval growth model and lacked other key biological aspects controlling the physical–biological interaction for sandeel larvae. They found that retention was larger in the southern parts of the North Sea than in the northern parts. Other more recent studies (Proctor et al. 1998; Gallego et al. 2004) have focused on a limited region of the North Sea shelf, the Orkney–Shetland Isles and the Scottish Isles. Using a barotropic hydrodynamic model on a coarse grid, Proctor et al. (1998) suggested that larval advection from Orkney to Shetland was important for Shetland recruitment in some years. Both studies tried to juxtapose virtual population analysis (VPA) recruitment data with transport indices, but both studies obtained only a moderate explanation of recruitment variability. In the present study, we will argue that a moderate correlation between recruitment and transport indices alone is what should be expected. With focus on closed-area effectiveness, Gallego et al. (2004) also suggested that some southern migration was possible between the Scottish Isles, but no comparison with recruitment observations were attempted.

In the present study, we provide an updated panoptic quantification of the central and southern North Sea transport patterns over a 35-year period using state-of-art three-dimensional (3D) hydrodynamic and individual-based modelling and show how to include transport indices into a coherent, process-oriented recruitment model framework.

Fig. 1. Sketch of coupled hydrodynamic and individual-based model (IBM) model SLAM (sandeel larval advection model).



Materials and methods

Based on the coupled ecosystem model framework ECOSMO (Schrum et al. 2003, 2006; Hochbaum 2004), a coupled hydrodynamic and individual-based model (IBM) has been developed for the early life stages (egg–larvae) of the lesser sandeel (Fig. 1). This model is called the sandeel larval advection model (SLAM).

Hydrodynamic model

The hydrodynamic module of ECOSMO (Schrum and Backhaus 1999; Schrum et al. 2006) is a free-surface, z -level model formulated on a staggered Arakawa C-grid. The model uses an approximate horizontal resolution of 5 nm and 5 m layers from the surface down to a depth of 40 m (and 8 m layers below 40 m depth). The model uses a terrain following lowest layer with spatially varying thickness. The Eulerian grid scale vertical turbulent diffusivity ($K(x,t)$) is used to describe larval dispersal in the IBM. Turbulent processes in ECOSMO are parameterized using an analytical k – ϵ approach, considering counteracting effects of local shear and stratification (Schrum 1997). The ECOSMO hydrodynamic model setup has been successfully validated against available observations (Janssen et al. 2001; Janssen 2002), particularly with respect to its performance in describing the interannual variability of hydrodynamic conditions. The detailed validations illustrated the model's ability to describe successfully seasonal and intraannual variability of hydrodynamic processes in the North Sea, hence justifying its employment in the study of hydrodynamic impacts on the North Sea ecosystem. For the present study, we used hydrodynamic model results from a previously performed long-term simulation from 1958–2004 (Schrum et al. 2003). The hydrodynamic fields from the ECOSMO model (currents, temperature, salinity, turbulence) are applied to the IBM as daily-averaged fields (for data-compression purposes).

Individual-based biological models

The biological states are updated daily, based on the physical environment. The biological part of the IBM con-

tains egg and larvae submodels. In the following sections, we will detail the submodels of the various aspects of sandeel early life history used in the present study. To label alternative composite larval models in a transparent way, we use the following designation template:

$$(1) \text{ Model} = \text{initialization_settlement}$$

Each considered aspect (initialization (e or h), settling (S40 or flx)) is associated with a model identifier (a tag) that corresponds to the actual submodel employed in the simulation; below we will elaborate the submodel alternatives in eq. 1. For instance, the reference model used below is labelled h_S40.

Initialization of larval-egg populations

We model the hatch process stochastically. The extended hatch period is hypothesized to be an important part of the sandeel life strategy, because larval recruitment success is believed to be strongly dependent on proper timing with secondary marine production (Wright and Bailey 1996). Strictly deterministic modelling of the hatch process will give a time-peaked hatch process if eggs are spawned at a specific time. This would not be in correspondence with field observations (Jensen 2001) or well-controlled laboratory experiments (Smigielski et al. 1984).

In our setup, tracers may be initialized in an arbitrary egg or larval state (or a mixed set). Eggs are immobile and demersal, whereas larvae are pelagic (but released at the bottom at hatch time). Eggs and larvae are initially positioned at suitable spawning grounds in the North Sea, as described below. Spawning grounds are assumed coincident with sandeel habitats, as no spawning migration has been observed. In this work, we will consider two opposite schemes for larval release to explore the influence of hatch period length on transport: first by releasing larvae directly on a single day (20 February) with an initial length L_0 at the sea bed; this initialization model is designated h in eq. 1. Secondly, we let the hatch time distribution be determined by an egg development model (giving an extended hatch period), as described below. Eggs are spawned demersally at a constant rate at 1 January; this initialization model is designated e in eq. 1.

The physically released larvae population is mathematically sampled by a set of representative tracers, each representing a fixed number of individuals (the ratio of real physical larvae per tracer need not be stipulated, as density effects are not addressed explicitly, only relative numbers matter).

Stochastic egg development model and hatching

In model e, the eggs are developed according to a hatch probability function, as parameterized from the egg maturation experiment of Smigielski et al. (1984) (Fig. 2b). The lines in Fig. 2 show smooth temperature fits to the statistical delimiters of the hatch process: beginning, median, and end, as function of temperature (T , in degrees Celsius):

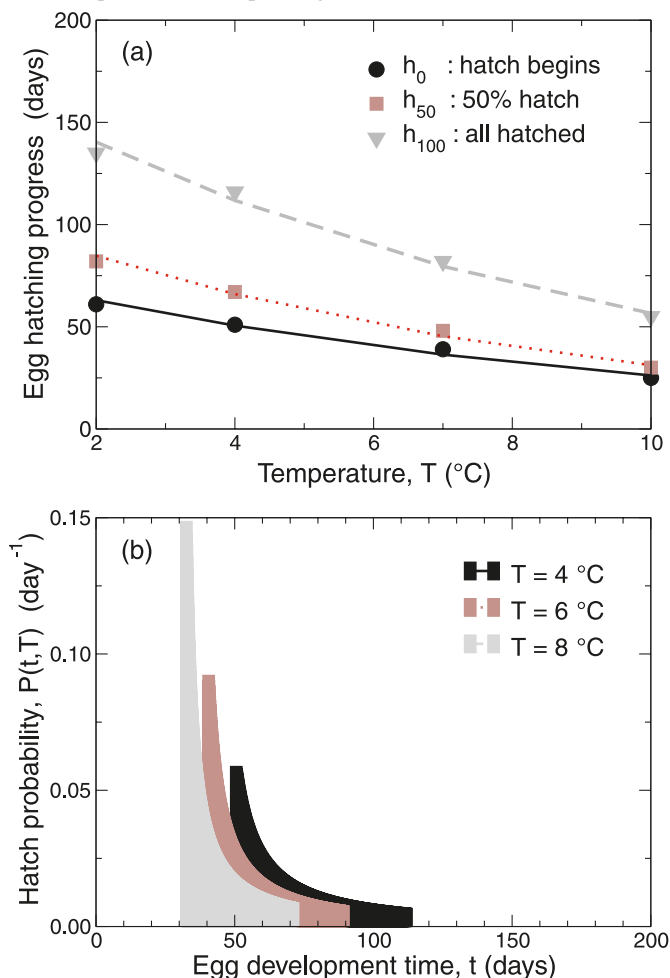
$$(2) \quad F(T) = Ae^{-kT}$$

where $F(T)$ is either hatch beginning ($b(T)$), hatch median ($m(T)$), or hatch end ($e(T)$). Parameters for hatch process

Table 1. Parameters for stochastic egg development model (model e) at hatch beginning ($b(T)$), hatch median ($m(T)$), or hatch end ($e(T)$).

	$b(T)$	$m(T)$	$e(T)$
A (days)	78.484	108.75	176.14
k (C^{-1})	0.10984	0.12488	0.11358

Fig. 2. Stochastic egg development model based on Smigielski et al. (1984). (a) When moving up vertically at a given temperature, the curves show the observed egg hatch progress (symbols are observation data points, lines are curve fits). (b) Continuous clutch hatch frequencies, corresponding to curves in (a).



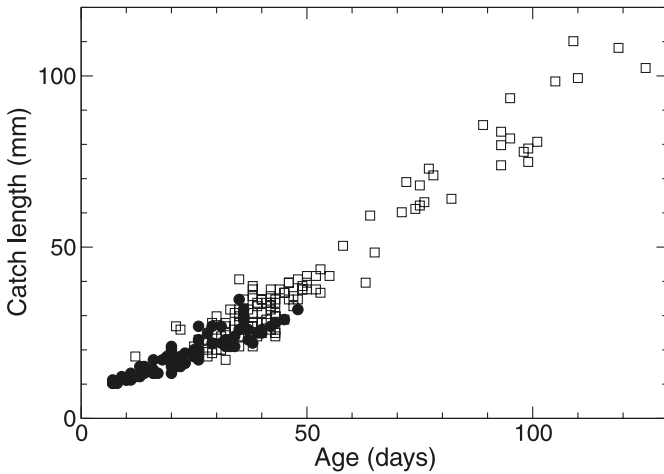
marker functions are found by standard nonlinear regression (Table 1).

These fits are mapped to an isothermal hatch probability function that depends parametrically on temperature (Fig. 2a):

$$(3) \quad Pr(t) = \begin{cases} 0 & t < b(T) \\ \frac{1}{n(T)} \frac{1}{t - g(T)} & b(T) < t < e(T) \\ 0 & t > e(T) \end{cases}$$

where t is day after spawning. Each egg is assigned a fixed relative growth rate, which reflects the idea that an embryo

Fig. 3. Age–length data for 1995 (solid circles) and 1996 (open squares) of pre- and post-metamorphosed larvae.



develops according to its genetic composition, as well as local physical parameters, like the oxygen tension (see, e.g., review by Kamler 2002), and local chemical transport coefficients. The relative magnitudes of these properties between eggs are strongly dependent on physical location of the individual egg; therefore the relative growth rate among eggs in the same cluster is assumed to be maintained, irrespective of fluctuations in the local physical environment. Technically, this corresponds to a stochastic nonlinear degree-day model. A deterministic linear degree-day model will display as a single hyperbola in Fig. 2a, or a hyperbolic envelope for a stochastic linear degree-day model. An ensemble of such eggs described by the development eq. 3 above will reproduce the hatch distributions in Fig. 2a, at a given temperature. In Appendix A, we give expressions for the auxiliary functions $n(T)$ and $g(T)$. The choice of $p_T(t)$ is the simplest asymmetric distribution that produces deviates directly from a mapping of a uniform distribution. We do not feel that the currently available hatch process data for the sandeel species warrants a more sophisticated parameterization. When eggs are hatched according to the stochastic egg model, each egg is automatically promoted to a larval individual starting at the seabed.

Larval growth models and data

The larval growth models accounts for the length growth of larvae as a deterministic, daily increment, according to

$$(4) \quad \frac{dL}{dt}(L, T) = \lambda(T) \left(\frac{L}{L_0} \right)^\gamma \left(1 - \frac{L}{L_\infty} \right)$$

The motivation for this is as follows. In the first term, temperature (T) acts as a proxy for bioenergetics effects (zooplankton production rate, metabolism, and activity level). In the second term, the larval length (L) accounts for the dominating size scaling effect in sandeel larval growth, which encompasses ontogenetic effects. The last term express growth saturation for $L \rightarrow L_\infty = 218$ mm (Macer 1966), due to increasing resting metabolism and reproduction investment. The effect of the last term becomes noticeable only after the size of metamorphosis, $L = L_m \sim 40$ mm (Wright and Bailey 1996; Jensen 2001). No memory effects in daily growth (like

Table 2. Growth parameters for larval growth (in units of $\text{mm}\cdot\text{day}^{-1}$).

Model	γ	λ_0	λ_1 (1°C)	Variance explanation (%)
1	0*	-0.642	0*	88.0
2	0*	-1.441	0.123	89.7
3	0.316	-1.725	0.136	90.1

Note: An asterisk (*) means that the parameter has been fixed to that value at model parametrization. Growth model 3 is the reference model used in simulations in this paper, unless otherwise stated.

larval condition) are included. The temperature modulation ($\lambda(T)$) is parameterized by a nonnegative factor as

$$(5) \quad \lambda(T) = e^{\lambda_0 + \lambda_1 T}$$

This simple growth model is parameterized from North Sea sandeel samples by MIK trawl and bottom dredge from 1995 and 1996 (Jensen 2001). Larval ages were obtained by individual otolith analysis (Wright 1993). The 1995 sample (80 larvae from seven locations) covers mostly premetamorphosed larvae, whereas the 1996 sample (124 sandeels from eight locations) covers mostly metamorphosed juveniles and settled sandeels. The spatial coverage of larval sampling stations in both years is frontal areas in the central and eastern North Sea. The larval age–length data from 1995 and 1996 plotted together appear to follow a common functional relation (Fig. 3).

Although sandeel larvae develop active swimming abilities before they metamorphose at a length $L_m \sim 40$ mm (Wright and Bailey 1996; Jensen 2001), we have assumed that they generally follow currents as passive tracers until they settle at the point of metamorphosis. The sensitivity of L_m is tested later.

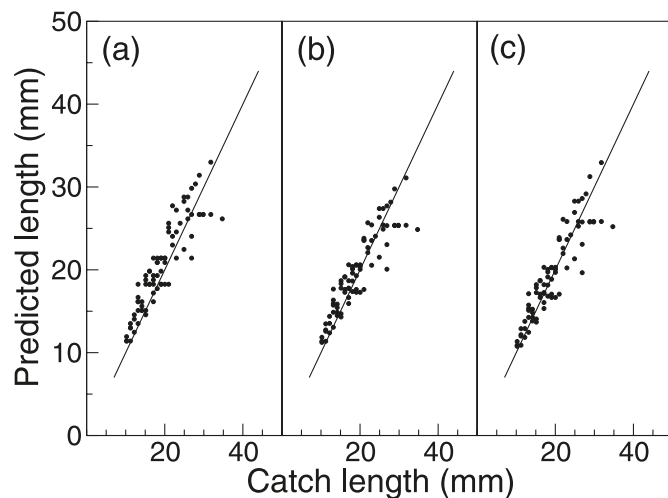
Premetamorphosis larval growth models

To parameterize the growth model (eqs. 4 and 5) above, we reconstruct the temperature history ($T_i(t)$) of individual larvae using the hydrodynamic backtracking scheme described recently (Christensen et al. 2007). Integrating eq. 4 above for each larva, we obtain a predicted length:

$$(6) \quad \tilde{L}_i = H(T_i(t_i^h < t < t_i^c), t_i^c, t_i^h; \gamma, \lambda_0, \lambda_1)$$

where t_i^c denotes catch day of larva i , and t_i^h is the hatch day (inferred from otolith reading). Notice that the first argument of $H(\bullet)$ above is the entire temperature history, not just a single temperature. By minimizing the sum of residuals between predicted larval lengths and observed larval lengths, we estimate growth parameters ($\gamma, \lambda_0, \lambda_1$) as a hierarchy of increasing complexity (Table 2). Model 1 (the null model) expresses constant growth, model 2 includes a temperature modulation term $\lambda(T)$, and model 3 additionally contains the allometric term with $\gamma \neq 0$. $L_0 = 7.73$ mm was inferred by extrapolation to hatch day in the figure using a quartic polynomial (this is similar to the largest size yolk sac larvae in samples from the western North Sea (Wright 1993)). We have fixed the parameter $L_\infty = 218$ mm (Macer 1966) when fitting data (Fig. 3), as it is of minor importance for larval growth (because $L_m \ll L_\infty$), but L_∞ adds a little convexity to the growth curve. We notice

Fig. 4. Comparison of observed and predicted larval length at catch using growth models 1–3 in combination with individual back-tracking: (a) growth model 1; (b) growth model 2; and (c) growth model 3. The line in each figure corresponds to perfect agreement with observed–predicted larval length.



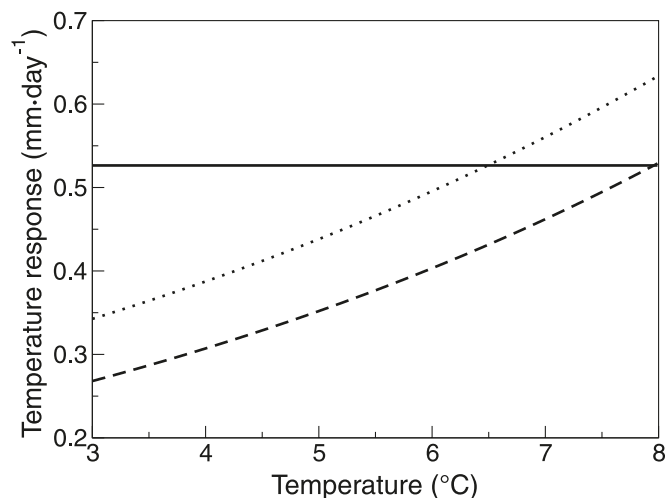
that the allometric term with $\gamma \neq 0$ becomes more important (sensitive) if growth in the postsettlement larval phase is considered.

The null model 1 (constant growth speed) already explains a very high degree of the data variance, leaving little room for improvement. Adding temperature and allometric effects may explain 20% of the residual variance only. Here, for premetamorphosed larvae, the temperature effects are relatively most important. This finding of a weak temperature influence is in accordance with Jensen (2001), who approached the problem indirectly via the correlation between otolith and larval growth. Here we confirm that indirect conclusion, considering the entire larval life history.

The variance structure in the residuals between the predicted and observed larval lengths (Fig. 4) is apparently the same in all models, supporting the statement that inherent individual variation and local environmental conditions beyond temperature influence is needed to account for the remaining residual variance. In the rest of this paper, we take growth model 3 as a reference model, which is used in all presented simulations, unless otherwise stated.

The temperature response functions $\lambda(T)$, inferred from the correlation between temperature track records and larval growth show that growth increases weakly with temperature (Fig. 5). The temperature derivative of the growth rate is of the order of $0.1 \text{ mm}\cdot\text{day}^{-1}\cdot\text{K}^{-1}$, in excellent overall agreement with Baistrocchi and Gallego (Baistrocchi 2003; Gallego et al. 2004), who estimated $0.13 \text{ mm}\cdot\text{day}^{-1}\cdot\text{K}^{-1}$ from another data set in a linear growth–temperature regression. Similarly, the net larval growth is within 15% in the temperature regime relevant to presettled sandeel larvae. In a tank experiment for *Ammodytes americanus*, Smigielski et al. (1984) also found a positive temperature derivative of the order of $0.03 \text{ mm}\cdot\text{day}^{-1}\cdot\text{K}^{-1}$. Correcting for the fact that the absolute growth rate of this reared species sample grew at approximately one-quarter the overall speed of the displayed *Ammodytes marinus* sample, our temperature derivative is in accordance with their estimate. We note that part of the tem-

Fig. 5. Temperature response function $\lambda(T)$ for growth models 1–3: growth model 1, solid line; growth model 2, dotted line; growth model 3, broken line.



perature response is likely indirect, via increasing secondary production with increasing temperature. Finally, we want to emphasize that generally determining the optimal separation of temperature response $\lambda(T)$ and the length scaling γ is difficult because seasonal temperature variation and larval length are strongly correlated. Currently, the growth model does not address explicitly density effects (food competition, cannibalism), although they are believed to affect recruitment on a population scale (Arnott and Ruxton 2002).

Larval premetamorphosis behavioural models

Horizontally, the larvae are described as passive drifters, with no explicit active vertical or horizontal migratory behaviour. Vertically, the dominant dispersal mechanism in the North Sea is turbulent diffusion, due to subgrid processes, coupled with current layer shear. The larvae move vertically in the water column according to a random walk (RW) process, with local step lengths reproducing local Eulerian field dispersal rates, which are proportional to the square root of the local diffusivity $K(x, y, z, t)$. This is modelled according to the following scheme (Visser 1997):

$$(7) \quad dR = \frac{\partial K(z)}{\partial z} h + u \sqrt{6h \cdot K \left(z + \frac{h}{2} \frac{\partial K(z)}{\partial z} \right)}$$

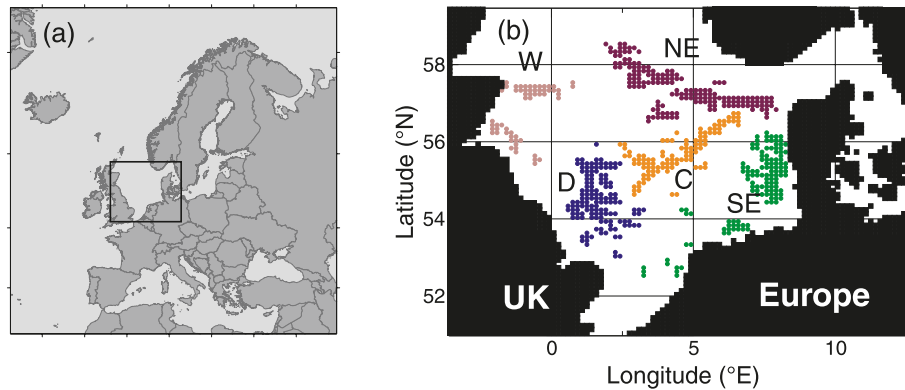
where dR is a vertical RW step, h is the RW time step, and u is a uniform random number in $[-1, 1]$. This RW process mirrors the Eulerian process for small time steps h :

$$(8) \quad \frac{\partial c}{\partial t} = \frac{\partial}{\partial z} \left(K \frac{\partial c}{\partial z} \right)$$

where $c(z, t)$ is the concentration of tracers. Encounter theory (e.g., in Fiksen and MacKenzie 2002) demonstrates biological advantages of actively selecting turbulence levels; this may be modelled by another gradient-driven term in eq. 7, similar to the first term in this eq. 7.

The boundary condition $dK(x, y, z)/dz = 0$ is imposed vertically at the surface and bottom to avoid artificial aggregation of tracers at the surface or bottom of the water column.

Fig. 6. (a) Study area shown as inlet. (b) Suitable sandeel banks in the central and southern North Sea divided into five major systems (s5). The bank systems are designated as shown in the figure: W, SE, D, C, and NE, which defines the enumeration order in the rest of the paper.



The simulations were performed with a time step $h = 30$ min using Euler forward integration. It was tested whether higher-order horizontal integration schemes (second-order Runge–Kutta) changed tracer trajectories, but the trajectories changed negligibly for $h = 30$ min. Longer time steps in conjunction with higher-order horizontal trajectory integration was not attempted, as this would imply large vertical jumps due to the stochastic modelling of turbulent dispersal. If tidal cycles were not averaged out of the hydrographic data, higher-order horizontal trajectory integration would be necessary to obtain accurate trajectories. In all presented spatial simulations, we used in total 600 000 RW tracers, which is sufficient for the current habitat resolution level and biological applications.

Sandeel habitats and settlement

During night and cold seasons with low zooplankton abundance, sandeel bury in the sandy seabed to avoid predation. The suitable sandeel habitats in the central and southern North Sea have recently been mapped (Fig. 6b) from Danish fishery data (Jensen and Rolev 2004).

Demersal eggs hatch at these sandbanks, and later larvae settle at these sandbanks at the end of their drift period, where they measure $L_m \sim 40$ mm. If metamorphosed juveniles do not migrate (which has not been observed), drift patterns must match habitat distributions to get successful recruitment; this is a central hypothesis examined in the present paper. Larvae not in the vicinity of a suitable sandbank at $L \sim L_m$ are assumed lost, because larvae lose transparency at metamorphosis, which strongly enhances the predation susceptibility.

Mapped sandeel habitats have been projected onto horizontal ($5 \text{ nm} \times 5 \text{ nm}$) hydrodynamic cells, giving in total of 596 high-resolution habitat cells (the central and southern North Sea covers ~ 4200 cells, for comparison). To analyze patterns in population variability, these 596 high-resolution habitat cells are also clustered into five larger regional bank systems (Fig. 6b), and we denote this division $s5$ hereafter. Other more-detailed regional divisions are conceivable and well justifiable, but this generally places higher demands on our biological submodels, and assumptions and further large volumes of transport data tend to obscure the patterns present in the results. In particular, a much more fine-grained bank division may require a more detailed settle-

ment model than the simple one used in this work. It is likely that habitat choice happens gradually around the length of metamorphosis $L = L_m \sim 40$ mm. This uncertainty is absorbed by choosing a coarse-grained bank system definition, because it is only boundary cases that are affected by this uncertainty: the transport indices are unaffected by uncertainties in settlement positions as long as they are in the correct bank system. The lateral extent of our bank systems is typically larger than 100 km, which analysis of similarity in sandeel size distributions among fishing banks has indicated as the maximum distance of subpopulation mixing (H. Jensen, unpublished data). No swimming longer than 10 km has been verified (K. Popp Madsen, Danish Institute for Fisheries Research (DTU-Aqua), Charlottenlund Slot, DK-2920 Charlottenlund, Denmark, unpublished data), which corresponds to the extent of a hydrodynamic cell, which is the spatial resolution limit in our study. Kunzlik et al. (1986) also inferred only minor horizontal migration from recapture experiments.

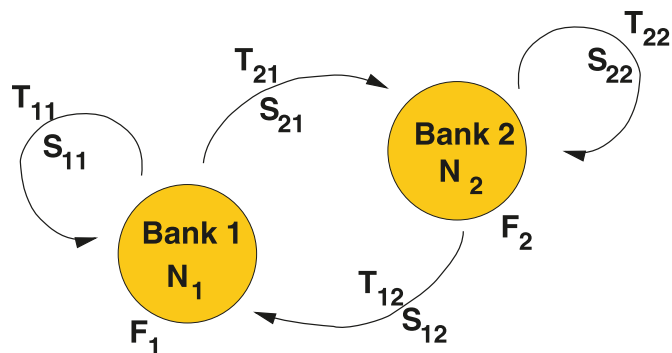
To assess the importance of a finite settling time window, we consider the two settling submodels. In the first model, we let larvae settle at length $L_m = 40$ mm (if they are at a suitable habitat); this settlement model is designated S40 in eq. 1. Secondly, we allow a finite settlement length interval, $37 \text{ mm} < L < 43 \text{ mm}$ (at first encountered habitat, if any); this settlement model is designated flx in eq. 1. A larger time window (model flx corresponds to ~ 11 days) for settlement is unlikely, because larvae lose transparency at metamorphosis and becomes highly susceptible to predation. Of course, the flx submodel gives higher transport success, and this has to be weighted by the extra mortality incurred because of longer drift time.

Transport

We wish to quantify transport between banks and retention on banks. Unfortunately, the concept of transport is often used casually, so to clarify the meaning of transport, as well as the dependence of simulation parameters, we give a rather formal definition of transport indices (Fig. 7), in the sense that we use it in Appendix B.

Hydrodynamic transport of matter in a given current field is a linear process. This means, firstly, that transported matter is proportional to the released amount of matter and, secondly, that transport from one point to another is

Fig. 7. Sketch of inter- and intra-bank transport dynamics: \mathbf{T} , transport index of passive drifters; \mathbf{S} , survival chance along transport paths; F , bank-specific egg productivity; N , adult sandeel population. Subscripts refer to banks.



independent of initial distribution of larvae. In other words, the net transport is a weighted superposition of point-to-point transport, where the weighting is the initial distribution of larvae. In Appendix B, we relate larval transport to the underlying hydrodynamic advection–diffusion fields and define larval transport indices \mathbf{T}_{ij}^{hV} from bank j to bank i that only depends on hatch distribution $h(t)$ and the biological settlement model V used (for notational simplicity, we drop superscripts h and V when this clear from the context). In addition to transport success, the larvae also needs to survive the transport, and we describe this conditional probability by \mathbf{S} ($0 < \mathbf{S} < 1$) as indicated (Fig. 7). Notice that bank retention is the diagonal terms \mathbf{T}_{ii} .

To analyze the transport structure, it is also convenient to consider three auxiliary contractions derived from the basic transport matrix \mathbf{T}_{ji} characterizing regional transport. The first is the outflow ω_i from bank i successfully reaching other banks:

$$(9) \quad \omega_i = \sum_{j \neq i} \mathbf{T}_{ji}$$

Adding bank retention to this gives the transport survival (or, in other words, the maximum potential for successful settling):

$$(10) \quad \rho_i = \omega_i + \mathbf{T}_{ii}$$

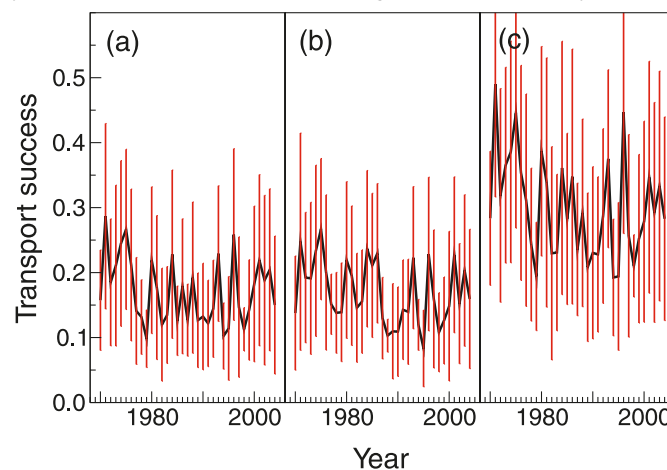
Finally, the inflow index from other banks to bank i is

$$(11) \quad \nu_i = \sum_{j \neq i} \mathbf{T}_{ij}$$

We want to emphasize that our transport indices \mathbf{T} , ω , and ν are independent of spawning intensity (and any uncertainty in spawning intensity assessment) because they describe the fraction of larvae that are successfully transported, due to linearity of transport, as discussed above.

Computationally, a transport matrix for a given year is obtained by releasing 600 000 tracers distributed homogeneously over all 596 hydrographic cells covering habitats and forward-tracking each of them by the appropriate biological submodel(s), as described above, until the juvenile stage; then the final positions are reprojected onto the 596 hydrographic cells covering habitats, and the raw 596×596

Fig. 8. Interannual variability in transport survival ρ for all central and southern North Sea banks for alternative biological models, corresponding to Table 2: (a), model h_S40; (b), model e_S40; (c), model h_flux. Average transport survival is indicated by the solid line. Spatial standard deviation (i.e., bank variability) for a given year, referred to $s5$ bank division (Fig. 6b), is indicated by bars.



transport matrix is aggregated into the 5×5 regional transport matrix, corresponding to the area division $s5$ (Fig. 6b). With a 5×5 regional transport matrix as target, a sampling of the transport integral (eq. B4) with in total 600 000 tracers is sufficient for precision needed for biological applications.

Conceptual spatial recruitment model

The transport indices defined above are cornerstones in computing annual recruitment from process-based modelling. Following the notation above (Fig. 7), the spatial explicit recruitment R_i^y in year y to bank i given by

$$(12) \quad R_i^y = \sum_j (T_{ij}^y S_{ij}^y F_j^y) N_j^y = \sum_j \alpha_{ij}^y T_{ij}^y N_j^y$$

This equation arises from simply adding successfully transported larvae. T_{ij}^y is the transport index defined above, F_j^y is the bank-specific fecundity (for year y at bank j), and S_{ij}^y is the conditional survival factor for an interbank transport (bank $j \rightarrow$ bank i), given successful transport from bank $j \rightarrow$ bank i . So, by construction, $0 < S_{ij}^y < 1$. S_{ij}^y quantifies additional larvae loss due to starvation and predation. In eq. 12, we also have introduced α_{ij}^y , which we denote the productivity index for later use, with a clear relation to underlying biological processes, which enables further research. In practice, when modelling most importantly fecundity F_j^y , one must keep track of, e.g., age composition at each bank j . This is most conveniently done by keeping N_j^y from previous years y , when solving iteratively eq. 12, and we suppress this from eq. 12 for notational simplicity.

Results

We have calculated a 35-year time series of interbank transport for the central and southern North Sea as described above. The transport survival ρ for model h_S40 (reference model) shows significant interannual and spatial variability (Fig. 8a). The spatial variability (bars in Fig. 8) is depend-

Table 3. Average ($\langle T \rangle$) and standard deviation (RMS(T)) of transport survival for the years 1970–2004 for alternative larval models.

	$\langle T \rangle$					RMS(T)				
	Scottish	SE	Dogger	Central	NE	Scottish	SE	Dogger	Central	NE
Model h_S40										
Scottish	0.055	0.000	0.000	0.000	0.000	0.017	0.000	0.000	0.000	0.001
SE	0.000	0.229	0.007	0.004	0.001	0.000	0.110	0.008	0.007	0.004
Dogger	0.013	0.000	0.264	0.019	0.000	0.017	0.000	0.088	0.034	0.000
Central	0.000	0.002	0.018	0.139	0.016	0.001	0.003	0.017	0.070	0.013
NE	0.029	0.007	0.000	0.012	0.041	0.035	0.010	0.000	0.015	0.023
Model e_S40										
Scottish	0.061	0.000	0.000	0.000	0.001	0.013	0.000	0.000	0.000	0.005
SE	0.000	0.225	0.008	0.004	0.001	0.000	0.107	0.011	0.007	0.005
Dogger	0.013	0.000	0.255	0.013	0.000	0.016	0.001	0.086	0.020	0.000
Central	0.001	0.002	0.019	0.135	0.011	0.003	0.004	0.013	0.076	0.010
NE	0.022	0.006	0.000	0.015	0.059	0.036	0.009	0.001	0.014	0.039
Model h_flx										
Scottish	0.112	0.000	0.000	0.000	0.001	0.029	0.000	0.002	0.000	0.003
SE	0.000	0.348	0.018	0.010	0.003	0.000	0.164	0.019	0.018	0.010
Dogger	0.022	0.000	0.420	0.034	0.000	0.027	0.001	0.117	0.056	0.000
Central	0.001	0.005	0.040	0.259	0.035	0.002	0.007	0.036	0.118	0.028
NE	0.057	0.023	0.000	0.028	0.086	0.066	0.034	0.000	0.032	0.044

Note: Rows and columns are indexed according to the regional division in Fig. 6b. Columns indicate starting bank system, whereas rows indicate transport destination.

ent, of course, on bank system partitioning, and the variability bars are based on the five major bank systems ($s5$) defined above (Fig. 6b). However, the average transport survival (Fig. 8, solid lines) is less sensitive to bank definition. The average transport success ($\langle \rho \rangle$) for this model is 17%, and the interannual standard deviation (RMS(ρ)) is 9.5%. The large spatial heterogeneity in the transport success stresses that spatial explicitness is necessary to approach robust recruitment models for North Sea sandeel larvae when comparing with eq. 12. For instance, in 1997, larvae starting on some bank systems only had 5% transport success, whereas other larvae of other subpopulations in 1997 had ~25% transport success. To compare $\langle \rho \rangle$ directly with VPA recruitment estimates would be premature, because the productivity index α_{ij} and population distribution time series N_j^y in eq. 12 also must be known to assess the recruitment. However, having the recent years of recruitment failure in mind, note that the time series (Fig. 8) does not reveal any recent climate change impacts on sandeel transport indices.

Transport structure

Statistical analysis of transport matrices and parameter sensitivity

We see that the overall trends and magnitudes in average transport indices are relatively robust toward reasonable changes in submodels that we have considered (Table 3) where the transport matrices T_{ij} corresponds to the $s5$ bank system (Fig. 6b). The transport matrices are quasi-diagonal (i.e., regional retention terms dominates). The region 3 (Dogger area) average transport retention dominates in all cases, of the order of 0.3.

The corresponding 35-year time series of transport sur-

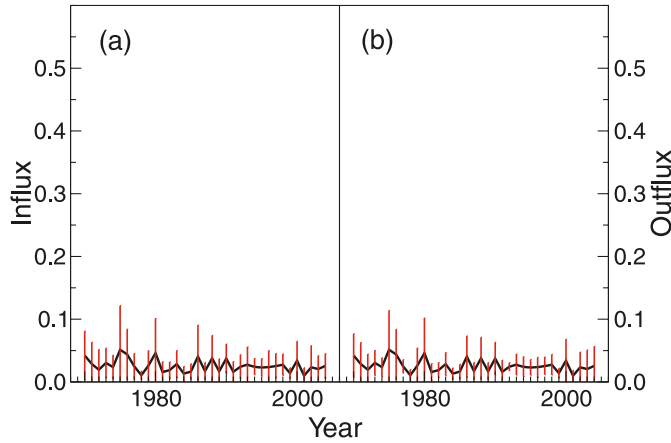
vival ρ for the alternative models also show significant interannual and spatial variability (Figs. 8b, 8c). Comparing the influence of extended hatch period with a single, fixed hatch day on transport success (Table 3), we see that no systematic influences are evident, only small scattered differences, e.g., the transport minimum in h_S40 is higher compared with e_S40, whereas e_S40 has an extended period around 1990 with low transport success.

The model with flexible settling schedule (flx) has a generally higher level of transport survival (30%), but this is just a multiplicative scaling, which does not change qualitative predictions: the relative transport success between years corresponds to that in other models. The higher general level of transport success will, at least partly, be compensated for by increased mortality resulting from increased drift time. We will return to this issue in the discussion. Comparing simulations with growth models 1, 2, and 3 (Table 2), we see only marginal differences in all results, consistent with the comparable residual variance levels in growth models 1, 2, and 3 (Table 2). Therefore we report only results corresponding to growth model 3 in this paper.

To summarize, although some minor differences are present in the variance structure, it is seen that the interannual variability is also agreed on between model options considered: all models agree on which years are good and bad transport years, again demonstrating the point that the transport patterns are robust towards model choices.

It is clearly seen that larval influx and outflux constitute a minor part of the net survival (Fig. 9); this is a general pattern that holds across models and years. Some years of high transport success, such as 1975 and 1980, also display high inflow (ω) and outflow (ν), but later years, such as 2001, display negative covariation with retention. That retention dominates the survival is very dependent on how bank sys-

Fig. 9. (a) Inflow index ν for $s5$ banks; (b) outflow index ω shown as time series averaged over banks for reference model h_S40 . Bank variability referring to $s5$ bank division in Fig. 6b is indicated by bars.



tems are defined: defining smaller bank systems generally shifts the reason for transport success from retention to successful influx and outflux. However, the net survival is relatively insensitive to how banks are aggregated into bank systems.

Spatial and temporal covariation in transport matrices

We have also tested the transport indices for spatiotemporal covariance patterns by evaluating the lagged pair covariance estimator:

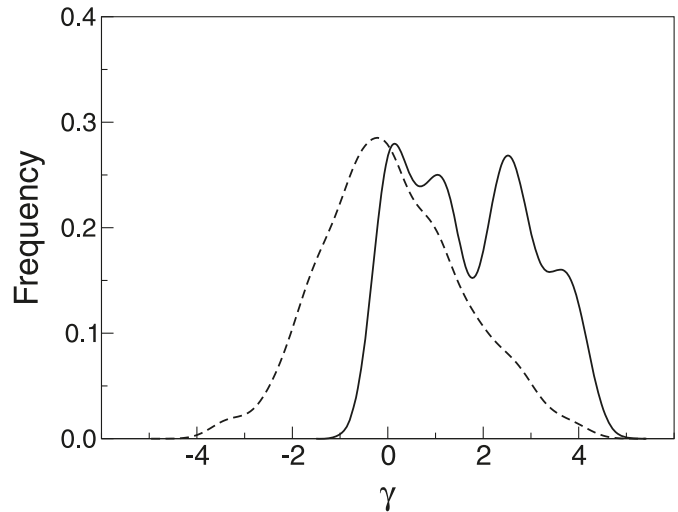
$$(13) \quad C_{ij,kl}^m = \frac{1}{1 + Y_1 - Y_0 - m} \sum_y (T_{ij}^y - \langle T_{ij}^y \rangle_y) \times (T_{kl}^{y+m} - \langle T_{kl}^y \rangle_y)$$

for our generated time series of transport matrices covering years $Y_0 = 1970 \leq y \leq Y_1 = 2004$. Here m is time lag in years and brackets $\langle \dots \rangle_y$ indicate time average of the quantity in the bracket. It is seen that $C_{ij,kl}^m = C_{kl,ij}^{-m}$, so we consider only time lags $m \geq 0$, but all combinations of $\{ij; kl\}$. However, even with our coarse regional bank division $s5$ (Fig. 6b) containing five regions, an immense number of covariance possibilities exist, especially if large time lags m are also considered. Two classes of covariances are especially interesting: spatial covariance within the same year ($C_{ij,kl}^0$) and transport autocorrelation ($C_{ij,ij}^m$). To test the statistical significance of the transport covariances, we divided by the standard deviation $\sigma(C_{ij,kl}^m)$ of the estimator $C_{ij,kl}^m$ evaluated analytically for the null hypotheses that T_{ij}^y are independent stochastic variables (in this case, the estimator $C_{ij,kl}^m$ can be expressed in terms of second and fourth moments of the transport matrices, which can be estimated directly from the transport matrix time series). We term this the excess covariance:

$$(14) \quad \gamma_{ij,kl}^m = \frac{C_{ij,kl}^m - \langle C_{ij,kl}^m \rangle}{\sigma(C_{ij,kl}^m)}$$

Additionally, because of the large number of covariance $\{ij; kl\}$ index combinations, the level of statistical significance must be adjusted down by the Bonferroni correction

Fig. 10. Distribution of excess covariance for reference model h_S40 : covariance of retention terms with time lag 0, solid line; distribution of all excess covariances with time lag 0 and 1 year, all pooled together, broken line. Distributions were broadened with $\gamma = 0.4$ to suppress sampling noise.



to avoid statistical type II errors (false positive statistical test compared with the null hypothesis). People often use less conservative measures than the Bonferroni correction to screen statistical type II errors, but we do not want to enter this dubious path of arguing statistical acceptance limits without indisputable reasons. All covariances ($m = 0, 1$) and all $\{ij; kl\}$ were tested for statistical significance.

The excess distribution for all covariances (Fig. 10, broken line) is close to a normal distribution, indicating that the bulk the covariances $\{C_{ij,kl}^m\}$ are indeed explained as random fluctuations. A single class of covariances significantly exceeded 1% Bonferroni corrected significance level: the $m = 0$ positive correlation between bank retention (Fig. 10, solid line). This was observed across all tested models. The most significant covariation was between SE–Dogger and Dogger–central retention. A single negative correlation involving interbank transport emerged: SE–Dogger and Dogger retention, which were marginally significant. These findings make sense from the point of view that retention and interbank transport are complementary, to some extent, if the net transport survival does not vary too much. So if interbank transport is low, retention should be high and correlated over many regions. Interbank transport is less correlated, because many coupling correlations exist. The complementary interpretation is also emphasized by the negative SE–Dogger and Dogger retention covariation.

In summary, in the time series underlying this work, the spatiotemporal covariances of matrices T_{ij}^y are generally weak or nonexistent. Only retention elements show some positive covariation. Therefore, at a first coarse level of modelling, we conclude that it is a reasonable approximation to consider T_{ij}^y as independent stochastic variables from a nonnegative distribution with average and standard deviation as given (Table 3). The next step in stochastic modelling is to include the retention covariation, which can be implemented relatively easily.

Discussion

Our transport indices T_{ij}^y may be applied directly into sandeel recruitment models, as demonstrated above. First, however, the spatial and interannual heterogeneity of F_j^y and S_j^y must be estimated to produce realistic recruitment predictions. A realistic parameterization of F and S is beyond the scope of the present study, but we would like to add a few remarks aiding further investigations in this direction. A very interesting question is whether transport indices alone are able to explain recruitment variability (i.e., we may assume $\alpha = S \cdot F$ is relatively constant in eq. 12). This question may be addressed at a very crude level, if we consider the recruitment per standing stock number (SSN): $r = R/N = \alpha T$. The final International Council for the Exploration of the Seas (ICES) ACFM sandeel assessment (1983–2004) (ICES 2005) shows that recruitment per SSN displays the relative variability $\sigma(r)/\langle r \rangle \sim 0.5$. Using standard rules of probability calculus and our results in this paper, we obtain the rough order-of-magnitude estimate:

$$(15) \quad \frac{\sigma(\alpha)}{\langle \alpha \rangle} \approx \frac{\sigma(T)}{\langle T \rangle} \approx 0.3$$

where an adult total average mortality $z \sim 1.5 \cdot \text{year}^{-1}$ from MSVPA (ICES 2007) has been applied. In other words, productivity α and transport T are about equally important in determining recruitment variability, and to make quantitative recruitment predictions, both α and T must be addressed. This simple observation also explains why previous North Sea transport studies have not been able to consistently explain recruitment variability. We also want to stress that an implication of eq. 12, the spatial heterogeneity in transport success, and the correlation analysis of T_{ij}^y time series is that deterministic recruitment models must be spatially explicit to approach goals of being quantitatively reliable. From eq. 12, we may sum up the total stock–recruitment:

$$(16) \quad \begin{aligned} R^y &= \sum_{ij} \alpha_{ij}^y T_{ij}^y N_j^y \\ &= \left(\sum_{ij} \alpha_{ij}^y T_{ij}^y \frac{N_j^y}{N_{SSN}^y} \right) N_{SSN}^y \\ &= Q^y N_{SSN}^y \end{aligned}$$

where Q^y is the (density-dependent) recruits per spawner. A nonspatial recruitment model requires that fluctuations in α_{ij}^y , T_{ij}^y , and N_j^y are proportional, and there is no reasonable basis for expecting this, following our analysis in the previous section. Following traditional stock–recruitment models and imposing $Q^y = Q(N_{SSN}^y)$ leads to a stochastic function $Q(N_{SSN}^y)$, the variance of which ultimately limits the predictive power of the recruitment model. These considerations hold for sandeel and may be extended to other species for the same reasons.

In our formulation, any mortality schedule can be applied a posteriori to the transport calculation, which is a great advantage when comparing scenarios and assessing parameter sensitivity. A reasonable null model is to use a spatially uniform S^y , which is justified by the fact that the passive drift time of survivors is reasonably uniform, as implicated from

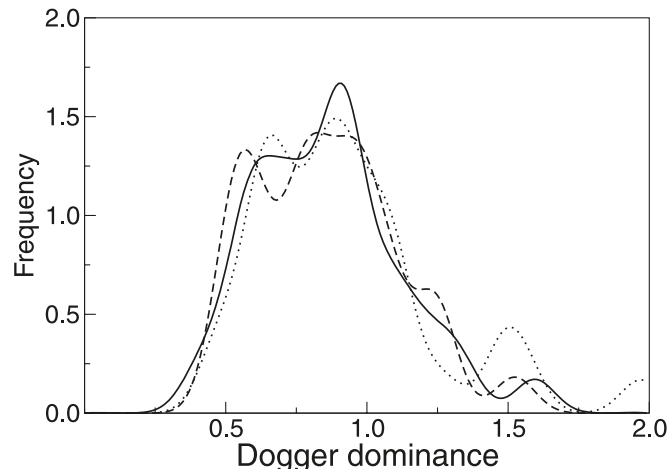
the variance analysis of growth data underlying the present study. A next step would be to overlap drift trajectories with temporal and spatially resolved effective predation fields. In this context, it would be interesting to assess the influence of herring, which is known to prey on sandeel larvae and early juveniles (Pommerantz 1981; Hopkins 1989; Last 1989). However, adult sandeel has also been identified as a main inhibitor on sandeel recruitment (Daan et al. 1990; Kimura et al. 1992; Arnott and Ruxton 2002). Whether this interaction is competition for food or habitat between larvae and adults or cannibalism is a question that is as yet unanswered.

We found that the temperature effect on sandeel growth was relatively moderate and of a magnitude consistent with other relevant studies of sandeel. It is important to realize that our conclusions pertain to survivors. We do not currently know much about the ones that starved along transport and the effect of starvation on survival, but this is necessary to determine the starvation component of S . Generic bioenergetic growth models (Letcher et al. 1996) stipulate that larvae die if they lose more than 25% somatic weight in starvation periods. Such conditions generate sharp windows of survival, when stochastic effects are included (e.g., small-scale patchiness), and therefore we have reason to believe that the larval sensitivities to ambient biological parameters are strong and complex, as it is difficult to determine the exact edges of the survival window from survivorship analysis. Because larvae possess elementary regulatory mechanisms (e.g., to keep on searching for food until satiated) and, at the same time, have hard biological limits (e.g., death when weight loss exceeds 25%), it is an interesting question how much survival is actually controlled by smooth spatial variations in ambient biological conditions, compared with inevitable small-scale fluctuations in ambient biological conditions.

Another issue for further investigation is the effect of active vertical and horizontal larval behaviour, including subdaily motion, such as diurnal migration (Jensen et al. 2003), where larvae appear to actively seek vertical layers with high zooplankton abundance in light periods. It is also an open question whether large-scale horizontal food gradients influence larval transport indirectly by biasing local food-seeking activity. Also, passive hydrodynamic mechanisms for frontal retention (Franks 1992) must be examined in closer detail for the North Sea. The significance of vertical migrations on horizontal transport has been exemplified for zooplankton in other areas (Queiroga and Blanton 2004). The cues for vertical migration could be tidal or ambient light signals. The importance of such hypotheses will be examined in future work, but unfortunately, it is not possible to address subdaily motion with the present hydrodynamic database, because physical fields are averaged to daily average fields. This would require a tidal current correction to the daily average fields in conjunction with a pattern of active subdaily motion.

An interesting finding in our study was that a flexible settlement schedule (settlement over a week) compared with a more tight settlement schedule gave the strongest increase in overall transport success (from 17% to 30%). However, this has to be balanced against a possible increased risk of predation (due to loss of transparency at metamorphosis). The

Fig. 11. Probability distributions of dogger area growth dominance over competing areas: model h_S40, solid line; model e_S40, dotted line; model h_flx, broken line. Dogger growth dominance indicated by the ratio between the largest non-Dogger eigenvalue (i.e., the corresponding eigenvector has its main weight on another region) and the eigenvalue belonging to Dogger. When the ratio is around 1, there is a propensity for “spatial blinking”.



exact risk increase is unknown, but it is reasonable to assume that it is on the scale of the mortality z experienced at that life stage. A rough estimate is $z \sim 0.07 \cdot \text{day}^{-1}$ (Wright and Bailey 1996). Adding this up to a week decreases the survival chance by 40%. So we have good reason to believe that the increased survival chance by flexible settling schedule is more or less cancelled by a corresponding decrease in conditional survival factor S . This observation strengthens the validity of our calculated transport indices. We have not considered the effect on transport success of spawning season width in the present study; however, in comparison with the minute effect of a prolonged hatch period (initialization model e versus model h), we believe that this will have a minor impact on the results. The same argument also holds for small changes in the offset of the hatch period.

In this paper, we have considered a relatively coarse regional division of the North Sea sandeel habitats. However, with the raw, high-resolution transport matrices \mathbf{T}_R (i.e., the 596×596 transport matrix) computed in this study, it is always possible to calculate the transport for any bank system definition alternative to $s5$ by a simple transformation:

$$(17) \quad \mathbf{T} = \mathbf{U}^t \mathbf{T}_R \mathbf{U} \boldsymbol{\pi}$$

which is derived from the transport integral definition (eq. B4). The matrix $\mathbf{U}_{ik} = 1$ if cell i is a member of bank k , and 0 otherwise. $\boldsymbol{\pi}$ is a diagonal matrix of priors, usually, e.g., the inverse of the number of cells in bank k . However, a significantly finer regional division requires an increased number of tracers to resolve transport between weakly connected regions properly, because of stochastic sampling noise.

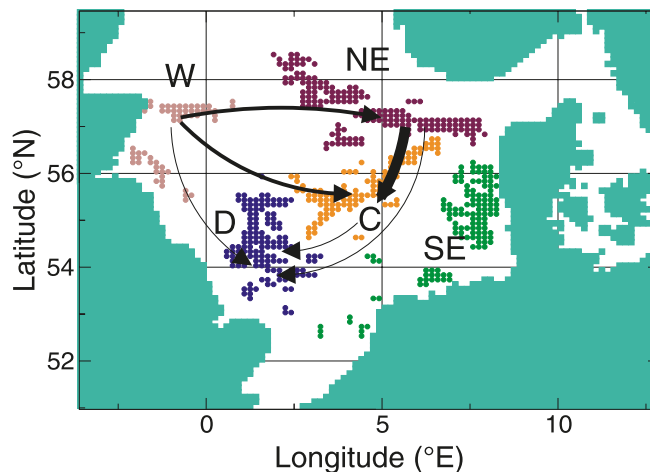
The considerations in the previous section focused primarily on statistical aspects of interbank transport. However, the quantitative and even qualitative demographic consequences are not obvious from this. For instance, stochasticity may trigger spatial or temporal resonances (McKane and Newman

Table 4. Expected travel times (Y , in years) between regions for model h_S40.

End	Start				
	1	2	3	4	5
1	—	>100	>100	>100	>100
2	44.9	—	41.7	42.3	43.0
3	18.8	49.5	—	18.7	23.9
4	12.3	31.5	20.5	—	5.4
5	16.7	35.9	45.8	33.9	—

Note: Columns are starting regions; rows indicate destination regions (see Fig. 6b).

Fig. 12. Most important interbank exchanges in the North Sea of sandeel larvae between $s5$ regions (Fig. 6b).



2005) in the population structure. A central element in this respect are the eigensolutions $\{\mathbf{w}_k, t_k\}$ of the transport matrices:

$$(18) \quad \mathbf{T} \mathbf{w}^k = t^k \mathbf{w}^k$$

The solutions to this equation describe population distribution modes being amplified by the transport structure. In the following, we index eigensolutions according to descending modulus $|t^k|$. Assuming that the productivity index α is spatially relatively weakly varying, the transport will amplify a spatial population distribution that is parallel to the leading eigenvector \mathbf{w}^0 , if the leading eigenvalue is well-isolated, i.e., $|t^0/t^1| \gg 1$. For all submodels considered in this paper, we find that the leading eigenvector, on average, has its main weight for the Dogger region (region 3). This is simply driven by the fact that this region has the largest retention on average. It is interesting to investigate the temporal stability of this, i.e., whether the stability flips occasionally. This is indicated by distribution functions of the ratio between the largest non-Dogger eigenvalue (i.e., the corresponding eigenvector has its main weight on another region) and the eigenvalue belonging to Dogger (Fig. 11). The distribution functions are generated from the eigensolutions of each transport matrix in our calculated time series. When the dominance ratio (Fig. 11) exceeds 1, the stability flips to another region. We see that there are some differences on this aspect between our considered submodels, but all considered models agree that in about two-thirds of the years, Dogger is dominating, whereas in about

one-third of the years transport favours other bank populations. Notice that these considerations are independent of the absolute values of α , to the extent that they are spatially homogeneous.

Finally, we want to discuss the bank connectivity structure implied by the transport matrices $\{\mathbf{T}\}$ in a little more detail. Essential properties are whether there exist isolated subpopulations, larval sources, or sinks. To answer these questions qualitatively, it suffices to focus on larval transport. We are not interested in the advective larval loss, i.e., larvae advected to areas without suitable habitats in which to settle. Therefore, we renormalize column-wise the transport matrix to turn it into a proper Markov matrix \mathbf{P} . This renormalization conserves the bank connectivity and relative efflux rates, which is essential for investigating dispersal time scales. Alternatively, only retention terms could be renormalized; both procedures give the same qualitative picture. The question of whether isolated subpopulations exist or not is then turned into a stringent question about whether \mathbf{P} is regular or not. A sufficient condition (e.g., Bartlett 1978) for regularity is that all elements of the matrix \mathbf{Q}^M ,

$$(19) \quad \mathbf{Q}^M = \sum_{n=1}^M \mathbf{P}^n$$

are nonzero for some $M > 0$. Loosely speaking, this condition tests whether it is possible to travel between all banks in, at most, M steps. (In other words, this condition also detects banks that are indirectly transport-connected, which may not be evident from the transport \mathbf{T} alone. To detect strict isolation of certain regions, we need only take $M = 5$ in eq. 19 above, as the longest nonoverlapping, indirect pathways connecting regions have then been exhausted.) We find that \mathbf{Q}^5 is strictly nonzero for all submodel combinations considered in this paper; however, \mathbf{Q}^M also indicates that regions are coupled to each other at different strengths. To elucidate this aspect, we introduce Y_{ij} , which is the expected time to travel from bank j to bank i , measured in years, when individuals are exchanged according to the Markov matrix \mathbf{P} . In Appendix C, we show that \mathbf{Y} can be calculated by the matrix equation:

$$(20) \quad \mathbf{Y} = (\mathbf{1} - \mathbf{I}) \cdot \{(\mathbf{1} + \mathbf{Y})\mathbf{P}\}$$

where $\mathbf{1}$ is a matrix of ones, \mathbf{I} is the matrix of unity, and the centered dot (\cdot) denotes an element-by-element matrix product.

The expected travel time (Table 4) corresponding to transport indices of the reference model h_S40 (Table 3) pertains to spreading time of, e.g., a passive genetic mutation (but time scales should be corrected for detection level). All models considered in this paper display the same approximate ordering and magnitude of the travel times (Fig. 12), even though some quantitative differences exist. Generally, s_5 regions are weakly coupled, the expected travel times being several years. Travel times from northern banks to central banks are smallest. The Scottish side banks act as sources for the rest of the North Sea (most dominantly the central and northern banks), the return times being extremely large. There is also a relatively large coupling between Dogger and central banks. The remaining expected travel times are typically of order of 30–40 years. The huge

return times to Scottish banks should not be taken very literally; these numbers are based on the average transport matrices — if interannual variations were included, these numbers would drop significantly, but still be large. Transport between weakly connected regions will be dominated by occasional bursts.

We also note that the exchange pattern is highly asymmetric (being directed). These predictions constitute an important contact point for population genetic investigations.

Acknowledgements

This work has been supported, in part, by EU FP6/SSP projects BECAUSE (contract no. 502482) and PROTECT (contract no. 513670) and the national DFFE/FIUF project “Fiskeriudsigt for tobis I Nordsøen på bankeniveau”. Insightful discussions with Uffe H. Thygesen on stochastic processes have been valuable and inspiring during the progress of the scientific work.

References

- Arnott, S.A., and Ruxton, G.D. 2002. Sandeel recruitment in the North Sea: demographic, climatic and trophic effects. *Mar. Ecol. Prog. Ser.* **238**: 199–210. doi:10.3354/meps238199.
- Baistrocchi, A. 2003. Modelling the spatial dynamics of sandeels in the western North Sea. M.Sc. thesis, Department of Statistics and Modelling Science, University of Strathclyde, Glasgow, Scotland, UK.
- Bartlett, M.S. 1978. An introduction to stochastic processes. Cambridge University Press, Cambridge, UK.
- Berntsen, J., Skagen, D.W., and Svendsen, E. 1994. Modelling the transport of particles in the North Sea with reference to sandeel larvae. *Fish. Oceanogr.* **3**: 81–91. doi:10.1111/j.1365-2419.1994.tb00051.x.
- Christensen, A., Daewel, U., Jensen, H., Mosegaard, H., St. John, M., and Schrum, C. 2007. Hydrodynamic backtracking of fish larvae by individual-based modelling. *Mar. Ecol. Prog. Ser.* **347**: 221–232. doi:10.3354/meps06980.
- Daan, N., Bromley, P.J., Hislop, J.R.G., and Nielsen, N.A. 1990. Ecology of North Sea fish. *Neth. J. Sea Res.* **26**: 343–386. doi:10.1016/0077-7579(90)90096-Y.
- Fiksen, Ø., and MacKenzie, B.R. 2002. Process-based models of feeding and prey selection in larval fish. *Mar. Ecol. Prog. Ser.* **243**: 151–164. doi:10.3354/meps243151.
- Franks, P.J.S. 1992. Sink or swim — accumulation of biomass at fronts. *Mar. Ecol. Prog. Ser.* **82**: 1–12. doi:10.3354/meps082001.
- Gallego, A., Heath, M.R., and Cook, B. 2004. The origin and destination of sandeel larvae sampled in the northern North Sea: biophysical modelling simulation results. *ICES CM 2004/P:09*.
- Hochbaum, U. 2004. Modelling of hydrodynamic influences in the life cycle of *Crangon crangon* in the North Sea. Diploma thesis at University Hamburg, Hamburg, Germany.
- Hopkins, P.J. 1989. Herring predation on fish eggs and larvae. *In* The North Sea ICES Early Life History of Fishes Symposium. Rapp. P.-V. Reun. Cons. Int. Explor. Mer, **191**: 459.
- International Council for the Exploration of the Seas. 2005. Report of the ICES Advisory Committee on Fishery Management, Advisory Committee on the Marine Environment and Advisory Committee on Ecosystems, 2005. ICES Advice. Book 6.
- International Council for the Exploration of the Seas. 2007. Report of the Working Group on the Assessment of Demersal Stocks in the North Sea and Skagerrak (WGNESSK), 5–14 September

- 2006, ICES Headquarters, Copenhagen, Denmark. ICES CM 2007/ACFM:35.
- Janssen, F. 2002. Statistical analysis of multi-year hydrographic variability in the North Sea and Baltic Sea. Validation and correction of systematic errors in a regional ocean model. Ph.D. thesis, Fachbereich Geowissenschaften, Universität Hamburg, Hamburg, Germany. [In German.]
- Janssen, F., Schrum, C., Huebner, U., and Backhaus, J. 2001. Validation of a decadal simulation with a regional ocean model for North Sea and Baltic Sea. *Clim. Res.* **18**: 55–62. doi:10.3354/cr018055.
- Jensen, H., Wright, P.J., and Munk, P. 2003. Vertical distribution of pre-settled sandeel (*Ammodytes marinus*) in the North Sea in relation to size and environmental variables. *ICES J. Mar. Sci.* **60**: 1342–1351. doi:10.1016/S1054-3139(03)00150-4.
- Jensen, H. 2001. Settlement dynamics in the lesser sandeel (*Ammodytes marinus*) in the North Sea. Ph.D. thesis, University of Aberdeen, Aberdeen, Scotland, UK.
- Jensen, H., and Rolev, A.M. 2004. The sandeel fishing grounds in the North Sea. Information about the foraging areas of the lesser sandeel *Ammodytes marinus* in the North Sea. Working document prepared for the EU project BECAUSE, Technical Report. Danish Institute of Fisheries Research, Charlottenlund Slot, DK-2920 Charlottenlund, Denmark.
- Kamler, E. 2002. Ontogeny of yolk-feeding fish: an ecological perspective. *Rev. Fish Biol. Fish.* **12**: 79–103. doi:10.1023/A:1022603204337.
- Kimura, S., Kishi, M.J., Nakata, H., and Yamashita, Y. 1992. A numerical analysis of population dynamics of the sand lance (*Ammodytes personatus*) in the eastern Seto Inland Sea, Japan. *Fish. Oceanogr.* **1**: 321–332. doi:10.1111/j.1365-2419.1992.tb00004.x.
- Kunzlik, P.A., Gauld, J.A., and Hutcheon, J.R. 1986. Preliminary results of the Scottish sandeel tagging project. ICES CM (Demersal Fish Comm.) 1986/G:7. pp. 1–6.
- Last, J.M. 1989. The food of herring, *Clupea harengus*, in the North Sea, 1983–1986. *J. Fish Biol.* **34**: 489–501. doi:10.1111/j.1095-8649.1989.tb03330.x.
- Letcher, B.H., Rice, J.A., Crowder, L.B., and Rose, K.A. 1996. Variability in survival of larval fish: disentangling components with a generalized individual-based model. *Can. J. Fish. Aquat. Sci.* **53**: 787–801. doi:10.1139/cjfas-53-4-787.
- Macer, C.T. 1966. Sandeels (*Ammodytidae*) in the south-western North Sea: their biology and fishery. Fisheries Investigations, Series 2, Vol. 24, No. 6. Ministry of Agriculture, Fisheries and Food, London, England.
- McKane, A.J., and Newman, T.J. 2005. Predator-prey cycles from resonant amplification of demographic stochasticity. *Phys. Rev. Lett.* **94**: 218102. doi:10.1103/PhysRevLett.94.218102. PMID:16090353.
- Pommerantz, T. 1981. Observation on the predation of herring (*Clupea harengus* L.) and sprat. *Rapp. P.-V. Reun. Cons. Int. Explor. Mer.* **178**: 101–109.
- Proctor, R., Wright, P.J., and Everitt, A. 1998. Modelling the transport of larval sandeels on the north-west European shelf. *Fish. Oceanogr.* **7**: 347–354. doi:10.1046/j.1365-2419.1998.00077.x.
- Queiroga, H., and Blanton, J.O. 2004. Interactions between behaviour and physical forcing in the control of horizontal transport of decapod crustacean larvae: an overview. *Adv. Mar. Biol.* **47**: 107–214. doi:10.1016/S0065-2881(04)47002-3.
- Schrum, C. 1997. Thermohaline stratification and instabilities at tidal mixing fronts. results of an eddy resolving model for the German bight. *Cont. Shelf Res.* **17**: 689–716. doi:10.1016/S0278-4343(96)00051-9.
- Schrum, C., and Backhaus, J.O. 1999. Sensitivity of atmosphere-ocean heat exchange and heat content in the North Sea and the Baltic Sea. *Tellus Ser. A.* **51**: 526–549.
- Schrum, C., Siegmund, F., and St. John, M. 2003. Decadal variations in the stratification and circulation patterns of the North Sea. Are the 90's unusual? In ICES Symposium of Hydrobiological Variability in the ICES area 1990–1999. *ICES Mar. Sci. Symp.* **219**: 121–131.
- Schrum, C., Alekseeva, I., and St. John, M. 2006. Development of a coupled physical-biological ecosystem model ECOSMO. Part I. Model description and validation for the North Sea. *J. Mar. Syst.* **61**: 79–99. doi:10.1016/j.jmarsys.2006.01.005.
- Smigielski, A.S., Halavik, T.A., Buckley, L.J., Drew, S.M., and Laurence, G.C. 1984. Spawning, embryo development and growth of the American sand lance *Ammodytes americanus* in the laboratory. *Mar. Ecol. Prog. Ser.* **14**: 287–292. doi:10.3354/meps014287.
- Visser, A.W. 1997. Using random walk models to simulate the vertical distribution of particles in a turbulent water column. *Mar. Ecol. Prog. Ser.* **158**: 275–281. doi:10.3354/meps158275.
- Winslade, P. 1971. Behavioral and embryological studies on the lesser sandeel *Ammodytes marinus* (Raitt). Ph.D. thesis, University East Anglia, Norwich, UK.
- Wright, P. 1993. Otolith microstructure of the lesser sandeel, *Ammodytes marinus*. *J. Mar. Biol. Assoc. U.K.* **73**: 245–248.
- Wright, P., and Bailey, M. 1996. Timing of hatching in *Ammodytes marinus* from Shetland waters and its significance to early growth and survivorship. *Mar. Biol. (Berl.)*, **126**: 143–152. doi:10.1007/BF00571386.

Appendix A. Parameterization of hatch probability function

At a given temperature T , the hatch process is characterized by three time scales, measured from the spawning point: $b(T)$ is the hatch beginning, $m(T)$ is the hatch median, and $e(T)$ is the hatch end point. Imposing normalization and median condition on the probability distribution eq. 3 gives

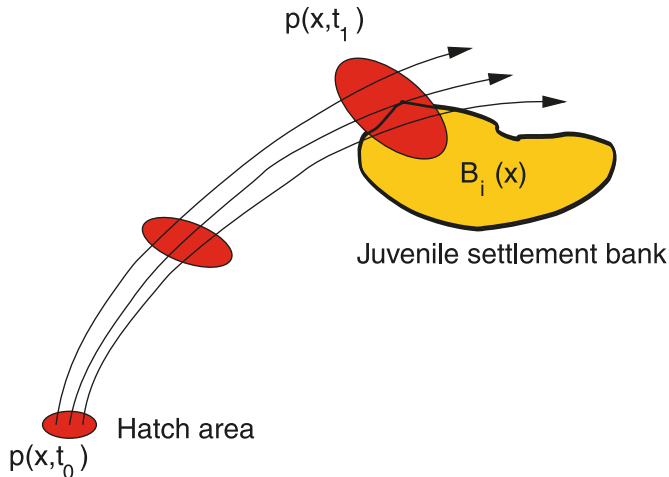
$$(A1) \quad g(T) = \frac{b(T)e(T) - m(T)^2}{b(T) + e(T) - 2m(T)}$$

$$(A2) \quad n(T) = \ln \frac{e(T) - \gamma(T)}{b(T) - \gamma(T)}$$

If the hatch distribution is skewed toward the hatch beginning, then $g(T) < b(T)$. In the special case in which the hatch probability becomes uniform, $m = (b + e)/2$, $\gamma(T)$ becomes large.

Appendix B. Definition and uniqueness of larval transport indices

The function describing the point-to-point transport is the so-called Greens function (or transport kernel), $G(x, t, x', t')$, which describes the probability of being transported from (x', t') to (x, t) . If we only included hydrodynamic advection, $G(x, t, x', t')$ would be peaked at the point (x, t) given by following the current line through x' at time t' until time t . If turbulent diffusion is included, $G(x, t, x', t')$ will be an expanding patch around the advection locus (x, t) (Fig. B1). The function $G(x, t, x', t')$ is completely and uniquely speci-

Fig. B1. Sketch of larval advection.

fied from the hydrodynamic advection–diffusion in the region of interest.

If we denote an initial larval patch distribution at time t_0 , $p(x', t_0)$, later at time t_1 , it has been transported into a patch distribution according to

$$(B1) \quad p(x, t_1) = \int G(x, t_1, x', t_0) p(x', t_0) dx'$$

Rather than mapping the full transport Greens function $G(x, t, x', t')$ (which is an eight-dimensional field), we focus on bank-to-bank transport described by $G(x, t, x', t')$. A bank i is described by a shape function $B_i(x)$, which is 1 if x is on

$$(B4) \quad \begin{aligned} \mathbf{T}_{ij}^V(t_0) &= \int \int dx dx' B_i(x) B_j(x') \int dt_1 G(x, t_1, x', t_0) V(t_1; x, x', t_0) \\ &= \int \int dx dx' B_i(x) B_j(x') \Omega^V(x, x', t_0) \end{aligned}$$

Thereby we have defined a transport index $\mathbf{T}_{ij}(t_0)$ that depends only on initial release time and the biological model V used; we also have derived rigorously the bank connectivity kernel Ω in terms of well-defined hydrodynamic and biological fields, as well as the exact parameter dependence of Ω .

If the hatch time is extended and described by a probability distribution $h(t)$, the net transport (over the season) is computed as a weighted integral, again due to linearity of transport:

$$(B5) \quad \mathbf{T}_{ij}^{hV} = \int \mathbf{T}_{ij}^V(t) h(t) dt$$

Appendix C. Expected travel time between bank systems

We want to calculate the average number of steps \mathbf{Y}_{ij} required to travel from sites j to i . The probability to travel from sites j to i in one step (in our context, the step unit is a year) is designated \mathbf{P}_{ij} , and especially important, the retention probability \mathbf{P}_{ii} can be nonzero. The expected travel time is most elegantly derived by a recursive argument:

the bank and zero elsewhere. The bank also has an area A_j (which can be obtained by integrating $B_j(x)$). Thus, if banks i and j are described by the shapes $B_i(x)$ and $B_j(x)$, respectively, then we describe the transport matrix \mathbf{T}_{ij} by

$$(B2) \quad \mathbf{T}_{ij}(t_1, t_0) = \frac{1}{A_j} \int \int G(x, t_1, x', t_0) B_j(x') B_i(x) dx dx'$$

The factor $(1/A_j)$ is a prior that assigns equal weights to all positions within the starting bank system j (which is a reasonable null hypothesis in the absence of more detailed knowledge and when the spatial extent of the bank system is small or moderate). For the regional splitting s_5 in the present work, $i, j = 1, \dots, 5$.

We let the settling time t_1 be determined by the biological clock, namely where the larvae reach the length of metamorphosis at $L \sim 40$ mm (Macer 1966; Reay 1970; Wright 1993). The probability that a larvae described by a biological model V attempts to settle at a given time t_1 depends on the position x and starting position and time (x', t_0) as

$$(B3) \quad P(t = t_1 | x, x', t_0) = V(t_1; x, x', t_0)$$

The settlement probability V depends on the transport history and is rather peaked in time. For simple biological models (like the one in this paper), V can be evaluated by path integral techniques, if the transport is computed by a Eulerian approach. We effectively compute V by a Monte Carlo approach when we run our combined hydrodynamic IBM. Inserting V into eq. B2, we obtain the settling probability on bank i from bank j as

$$(C1) \quad \mathbf{Y}_{ij} = \begin{cases} \sum_k (1 + \mathbf{Y}_{ik}) \mathbf{P}_{kj} & i \neq j \\ 0 & i = j \end{cases}$$

which expresses that the travel time is the weighted sum of direct and indirect travel paths times + 1. This recursive relationship can be written compactly as eq. 20, which is most conveniently solved iteratively (i.e., inserting a guess on right side, evaluating the equation, reinserting the result on right side, etc., until converged), but it can also be solved directly element by element, if desired. Notice that the travel time matrix \mathbf{Y} is not symmetric in general.

References

- Macer, C.T. 1966. Sand eels (*Ammodytidae*) in the south-western North Sea: their biology and fishery. Fisheries Investigations, Series 2, Vol. 24, No. 6. Ministry of Agriculture, Fisheries and Food, London, England.
- Reay, P.J. 1970. Synopsis of the biological data on the North Atlantic sand eels of the genus *Ammodytes*. FAO, Rome, Italy, Fisheries Synopsis No. 82.
- Wright, P. 1993. Otolith microstructure of the lesser sandeel, *Ammodytes marinus*. J. Mar. Biol. Assoc. U.K. **73**: 245–248.